An improved permeability evolution model and its application in fractured sorbing media

Gang Wang[a,b], Ke Wang[a,**], Shugang Wang[c,*], Derek Elsworth[d], Yujing Jiang[b]

[a] Shandong Provincial Key Laboratory of Civil Engineering Disaster Prevention and Mitigation, Shandong University of Science and Technology, Qingdao, 266590, China
[b] State Key Laboratory Breeding Base for Mine Disaster Prevention and Control, Shandong University of Science and Technology, Qingdao, 266590, China
[c] Geotechnical and Structural Engineering Research Center, Shandong University, Jinan, 250061, China
[d] Department of Energy and Mineral Engineering, Pennsylvania State University, University Park, PA, 16802, United States

ARTICLE INFO

ABSTRACT

In this paper, we consider fractured sorbing media (e.g., gas shale and coal bed methane reservoirs) as either dual porosity media comprising matrix-fracture or as triple porosity media comprising separate organic and inorganic matrix components and fractures. We accommodate the combination of mechanical deformation and desorption induced matrix shrinking in conditioning the evolution of fracture aperture and effective stress difference between each medium. These considerations result in an improved permeability evolution model (IPEM) for both dual porosity and triple porosity fractured sorbing media. Then we have simplified the model for triple porosity fractured sorbing media by reducing the geometry configuration from three dimensional to one dimensional, marked as SIPEM1. Specifically, SIPEM1 is a model simplified from the IPEM, and consider that when the size of the REV and the volumetric strain is small, replacing the volume with the side length of each layer medium in defining the model will bring relatively small error. This model is further simplified to SIPEM1-1 by assuming that the effective stress of each medium is the same. Then we have validated the models with field data. Finally, we compared prediction results from these models under different conditions. This study has found that IPEM is the most accurate model, especially for fractured sorbing media with a larger compressibility. SIPEM1-1 does not consider the difference of the effective stress of each medium and thus it is relatively less accurate in describing the evolution of permeability compared with SIPEM1 that considers this difference. This gap increases with the increase of permeability difference between fracture and matrix.

1. Introduction

Shale gas and coal bed methane reservoirs are becoming important as unconventional hydrocarbon resources (Middleton et al., 2017; Elsworth et al., 2016; Yuan et al., 2015). The evolution of porosity and permeability of shale gas/coal seam gas reservoirs are key factors controlling gas production, and these two parameters change dynamically during fluids production (Liu et al., 2011; Ma, 2015; Cui et al., 2018). Permeability evolution is related to changes in gas pressure in the reservoir when producing shale gas or coal bed methane. To be more specific, gas pressure drawdown in reservoirs triggers two competing processes. A reduction in gas pressure in the reservoir increases the effective stress, which compacts the reservoir and decreases the fracture aperture and thus permeability. Simultaneously, the adsorbed gas is desorbed from the matrix during production, and this process shrinks the matrix, widens fracture apertures and concomitantly enhances fracture permeability (Wang et al., 2012a; Wu et al., 2010a). Accurate description and quantification of these two opposing processes is the key to describing the evolution of permeability in fractured sorbing media.

An idealized gas shale or coal bed methane reservoir is shown in Fig. 1a. Such fractured sorbing reservoirs can be idealized as either dual porosity system, consisting of matrix and fracture as shown in Fig. 1b, or as triple porosity system, consisting of organic matrix, inorganic matrix and fracture as shown in Fig. 1c (Harpalani and Schraufnagel, 1990; Lu and Connell, 2007; Warren and Root, 1963; Zou et al., 2015; Sang et al., 2016; Gray, 1987). Previous studies have shown that the matrix, especially the organic component contributes mainly to the storage of gas, while the fracture system comprising networked micro-fractures, fissures, fractures, and faults is the primary gas flow migration channel (Gray, 1987). Robertson (2005) noted that cleat permeability could be as much as eight orders of magnitude larger than that of

---

* Corresponding author.
** Corresponding author.
E-mail addresses: sdwangke1115@163.com (K. Wang), sdgeowsg@gmail.com (S. Wang).
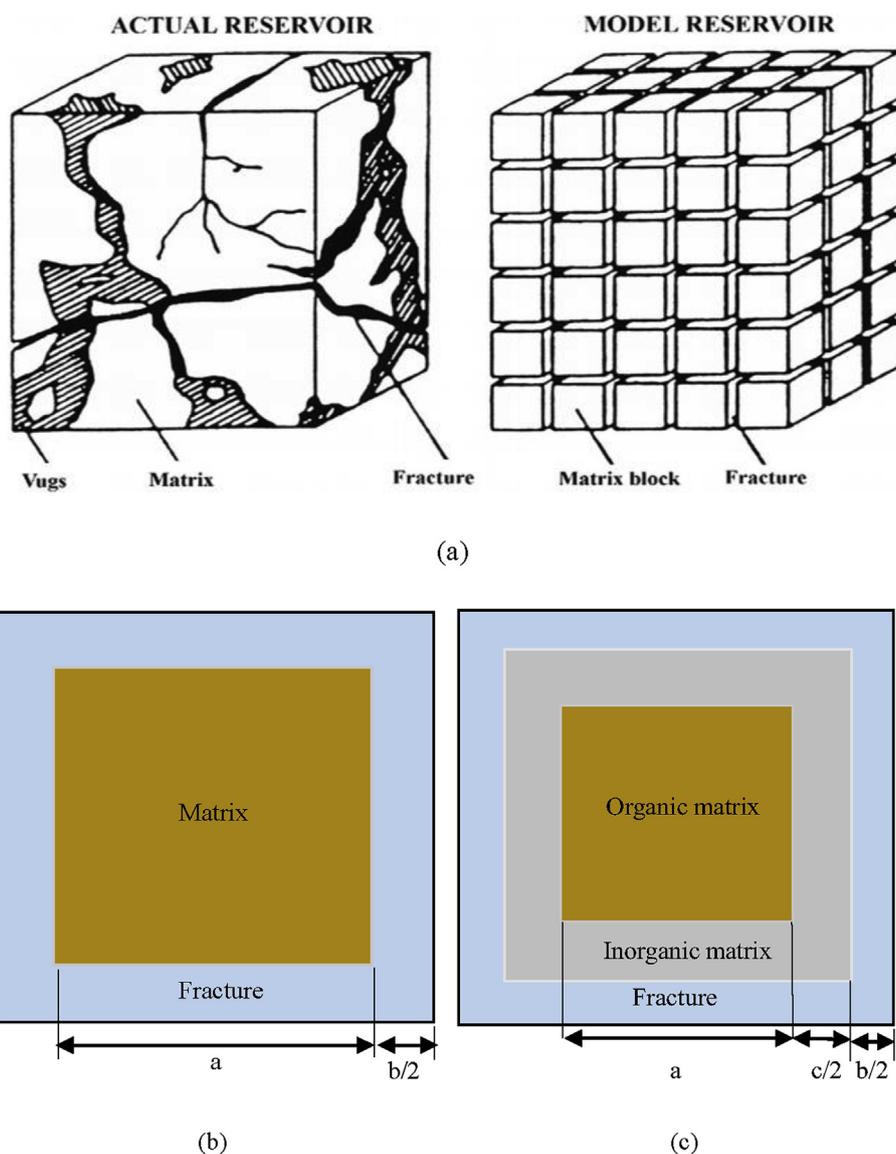
Fig. 1. Illustration of dual/triple porosity fractured sorbing media. (a) Idealization of a fractured sorbing media system (Warren and Root, 1963). (b). A two-dimensional representative element volume (REV) for the dual porosity media. (c). A two-dimensional representative element volume (REV) for the triple porosity media.

the matrix permeability. Therefore, it is most important to describe the evolution of fracture permeability to guide shale gas/coal bed methane extraction, together with controls on rate limiting diffusion from the matrix in defining release in storage. This is the focus of this work, including the role of both organic and inorganic components as separate phases.

1.1. Previous studies

Previous studies have described the evolution of permeability in fractured sorbing media. Sawyer et al. (1990) proposed a model assuming that fracture porosity is a linear function of changes in gas pressure and concentration. Seidle and Huitt (1995) developed a permeability model by considering the roles of coal-matrix swelling/shrinkage while ignoring the impact of coal compressibility. Palmer and Mansoori (1998) developed a permeability model incorporating the combined effect of elastic properties and gas sorption on the matrix strain. Robertson and Christiansen (2006) proposed a permeability model for coal and other fractured, sorptive-elastic media. Liu and Rutqvist (2010) considered a fracture-matrix interaction model during

coal-deformation processes and developed a coal permeability model. Wu et al. (2010a) assumed that the stress-induced strain is negligible with respect to the adsorption/desorption of coal-rock matrix and proposed a dual porosity dual permeability model of coal.

It is undeniable that the establishment of these models has significantly improved our understanding of the evolution of permeability in fractured sorbing media. However, most of these models do not consider all the physical processes involved during production, such as accurate representation of effective stress in matrix and fracture, fracture aperture, volumetric strain and so on. To be more specific, the effective stress in matrix and fracture is different in the production period because of the large difference in matrix permeability and fracture permeability that could potentially cause significant difference in gas pressure. Therefore, despite the stress-induced strain might be negligible with respect to the adsorption/desorption of the matrix, we should consider the difference of effective stress between matrix and fracture when developing permeability evolution model. Furthermore, because fracture aperture is very small, most of the previous study did not consider the impact of fracture aperture when calculating the volumetric strain of the fractured sorbing media. Finally, compared to

conventional gas reservoirs, coal reservoirs have larger compressibility (Liu et al., 2011). If the volumetric strain is not accurately calculated, permeability evolution model could certainly predict gas pressure evolution and production with large error. It is the purpose of this paper to accurately consider volumetric strain and to establish an improved permeability evolution model.

1.2. This study

This work represents fractured sorbing media as either dual porosity media (Fig. 1a) consisting of matrix and fracture (Fig. 1b), or triple porosity media consisting of organic matrix, inorganic matrix and fracture (Fig. 1c). The combined mechanical deformation and desorption-induced matrix shrinkage, adjusts fracture aperture and the effective stress difference between each medium to modify permeability in either form of the composite media. An improved permeability evolution model (IPEM) was established for fractured sorbing media through accurately expressing the volumetric strain of the REV.

This model was then simplified by modifying the model configuration from three dimensional to one dimensional, marked as SIPEM1. Specifically, SIPEM1 is a model simplified from the IPEM, and consider that when the size of the REV and the volumetric strain is small, replacing the volume with the side length of each medium will only create relatively small error. Then it was further simplified by assuming that the effective stress of each medium is the same, marked as SIPEM1-1. Then we have validated these permeability evolution models for fractured sorbing media consisting of triple porosity media using field data. Finally, to explore the differences among these models, we compared model results by using different input parameters for different cases. The flowchart used in this work is shown in Fig. 2.

2. Modeling

This section corresponds to the first part of the flowchart. An improved permeability evolution model for fractured sorbing media will be constructed. After that, we simplify the model for later comparative analysis.

2.1. Assumptions

In this work, the following basic assumptions are made:

1) Reservoir is isothermal, and gas viscosity is constant under isothermal conditions.
2) The reservoir is saturated with the ideal single-phase gas (CH_4).
3) Dual porosity media is composed of matrix-fracture, and triple porosity media is composed of organic matrix, inorganic matrix and fracture. Each medium is homogeneous and isotropic.
4) Gas adsorption/desorption follows the principle of Langmuir isothermal behavior, and this process only occurs in the matrix for dual porosity model, and the organic matrix for triple porosity model.
5) The deformation of the reservoir is assumed to be infinitesimal.

2.2. Improved permeability evolution model for dual porosity fractured sorbing media (IPEM)

In this section, we focus on the dual porosity fractured sorbing media (Fig. 1b). IPEM is established by accurately expressing the volumetric strain of the REV during gas production.

According to the effective stress principle for multi-porous media (Elsworth and Bai, 1992; Chen and Chen, 1999), the effective stress of the matrix and the fracture can be written as

$$\begin{cases} \sigma_{e1} = \sigma - (\alpha p_1 + \gamma p_f) \\ \sigma_{ef} = \sigma - \gamma p_f \end{cases} \tag{1}$$

where subscripted 1 represents the matrix, subscripted f represents the fracture; p represents gas pressure; σ represents the average principal stress that can be expressed as Eq. (2); α and γ are effective stress coefficients of matrix and fracture (Chen and Chen, 1999; Biot, 1941; Liu et al., 2017), respectively, and can be expressed as

$$\sigma = \sigma_{kk}/3 = (\sigma_{11} + \sigma_{22} + \sigma_{33})/3 \tag{2}$$

$$\begin{cases} \alpha = 1 - \dfrac{K}{K_1} \\ \gamma = 1 - \dfrac{K}{K_f} \end{cases} \tag{3}$$

where K_1 is the bulk modulus of the matrix, K_f is the bulk modulus of the fracture. K is the bulk modulus of the fractured sorbing media, defined by the elastic properties of the media as

$$K = \frac{E}{3(1 - 2v)} \tag{4}$$

where v is the Poisson ratio of the fractured sorbing media, E is the elastic modulus of the fractured sorbing media.

We assume that the length of the REV is s, then,

$$s = a + b. \tag{5}$$

The desorption induced shrinkage strain during gas production can be expressed as

$$\Delta \varepsilon_s = \varepsilon_s - \varepsilon_{s0} \tag{6}$$

where,

$$\begin{cases} \varepsilon_s = \dfrac{\varepsilon_L p_1}{p_L + p_1} \\ \varepsilon_{s0} = \dfrac{\varepsilon_L p_{10}}{p_L + p_{10}} \end{cases} \tag{7}$$

and ε_s is the sorption-induced strain with subscript 0 representing the initial state and given by the Langmuir isotherm (Langmuir, 2015).

After the initial equilibrium state, to accurately consider the effective stress in the matrix and the fracture, the volumetric strain of the REV can be expressed as

$$\Delta \varepsilon_v = \frac{a^3}{s^3 K_1} \Delta \sigma_{e1} + \frac{s^3 - a^3}{s^3 K_f} \Delta \sigma_{ef} - \frac{a^3}{s^3} \Delta \varepsilon_s. \tag{8}$$

In this equation, the first item on the right side is the degree of contribution of volumetric strain of matrix induced by the change of effective stress to the volumetric strain of the REV; the second item is the degree of contribution of volumetric strain of fracture induced by the change of effective stress to the volumetric strain of the REV; and the third item is the degree of contribution of shrinkage of matrix induced by the desorption.

Substituting Eq. (1) into Eq. (8), we can obtain the following equation

$$\Delta \varepsilon_v = \frac{a^3}{s^3 K_1} [\Delta \sigma - (\alpha \Delta p_1 + \gamma \Delta p_f)] + \frac{s^3 - a^3}{s^3 K_f} (\Delta \sigma - \gamma \Delta p_f) - \frac{a^3}{s^3} \Delta \varepsilon_s. \tag{9}$$

Therefore, the change of effective stress in the fracture can be rewritten as

$$\Delta \sigma - \gamma \Delta p_f = \frac{1}{\frac{a^3}{s^3 K_1} + \frac{s^3 - a^3}{s^3 K_f}} \left(\frac{a^3}{s^3} \Delta \varepsilon_s + \Delta \varepsilon_v + \frac{1}{s^3} \frac{a^3}{K_1} \alpha \Delta p_1 \right). \tag{10}$$

The change in effective stress induced fracture deformation can be obtained from

$$\Delta b = \frac{b}{3 K_f} \Delta \sigma_{ef} = \frac{b}{3 K_f} (\Delta \sigma - \gamma \Delta p_f). \tag{11}$$

The change of fracture porosity can be expressed as
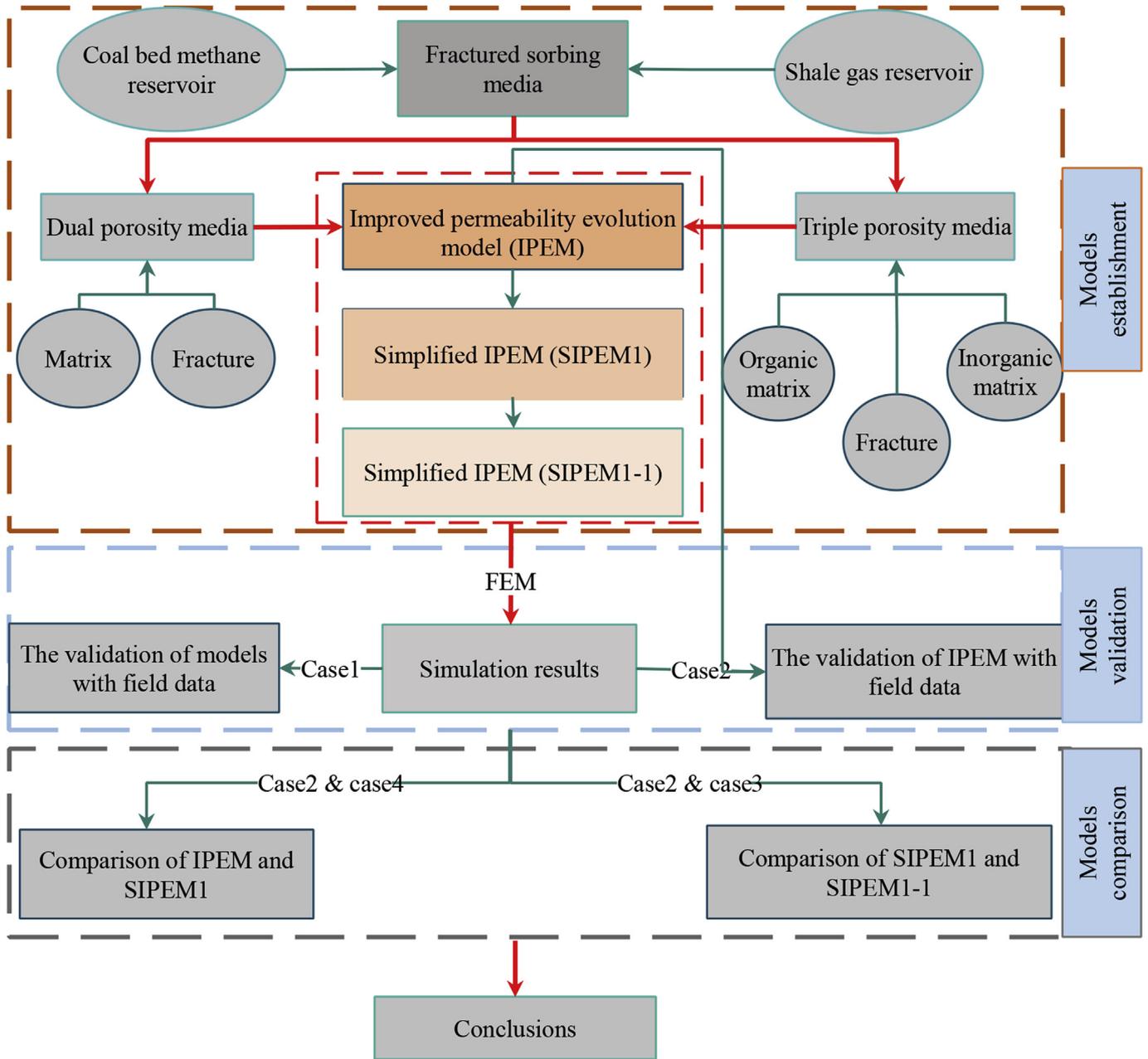
Fig. 2. The workflow used in this work.

$$\frac{\phi_f}{\phi_{f0}} = 1 + \frac{\Delta b}{b} = 1 + \frac{1}{3K_f} \frac{1}{\frac{a^3}{s^3 K_1} + \frac{s^3 - a^3}{s^3 K_f}} \left(\frac{a^3}{s^3} \Delta \varepsilon_s + \Delta \varepsilon_v + \frac{1}{s^3} \frac{a^3}{K_1} \alpha \Delta p_1 \right).$$

(12)

Based on the cubic Law (Chilingar, 1964), we can finally obtain the improved permeability evolution model (IPEM) for dual porosity fractured sorbing media as

$$\frac{k_f}{k_{f0}} = \left(\frac{\phi_f}{\phi_{f0}} \right)^3 = \left[1 + \frac{1}{3K_f} \frac{1}{\frac{a^3}{s^3 K_1} + \frac{s^3 - a^3}{s^3 K_f}} \left(\frac{a^3}{s^3} \Delta \varepsilon_s + \Delta \varepsilon_v + \frac{1}{s^3} \frac{a^3}{K_1} \alpha \Delta p_1 \right) \right]^3.$$

(13)

After established IPEM for dual porosity fractured sorbing media, next we develop the permeability evolution model for triple porosity fractured sorbing media.

2.3. Improved permeability evolution model for triple porosity fractured sorbing media (IPEM)

Shale reservoir can be also considered as a fractured sorbing media containing organic matrix, inorganic matrix, and fracture, as shown in Fig. 1c (Sang et al., 2016), where a, c and b are the length of the organic matrix, inorganic matrix, and fracture system, respectively.

The effective stress for triple porosity fractured sorbing media can be expressed as

$$\begin{cases} \sigma_{e1} = \sigma - (\alpha p_1 + \beta p_2 + \gamma p_f) \\ \sigma_{e2} = \sigma - (\gamma p_f + \beta p_2) \\ \sigma_{ef} = \sigma - \gamma p_f \end{cases}$$

(14)

where 1 represents the organic matrix, 2 represents the inorganic matrix, α and β are the effective stress coefficients of the organic matrix and the inorganic matrix, respectively. The effective stress coefficient for the inorganic matrix can be written as

$$\beta = 1 - \frac{K}{K_2}. \tag{15}$$

And the rest of the parameters are the same with those defined in the dual porosity model.

For triple porosity media, the length of the REV can be simplified as $s = a + b + c$, and the matrix side can be expressed as $l = a + c$.

Similar to the dual porosity model, the volumetric strain of the triple porosity media can be expressed as

$$\Delta \varepsilon_v = \frac{a^3}{s^3 K_1} \Delta \sigma_{e1} + \frac{l^3 - a^3}{s^3 K_2} \Delta \sigma_{e2} + \frac{s^3 - l^3}{s^3 K_f} \Delta \sigma_{ef} - \frac{a^3}{s^3} \Delta \varepsilon_s. \tag{16}$$

The items in the above equation are similar to that in Eq. (8), so these are not repeated here.

Substituting Eq. (14) into Eq. (16), we obtain

$$\Delta \varepsilon_v = \frac{a^3}{s^3 K_1} [\Delta \sigma - (\alpha \Delta p_1 + \beta \Delta p_2 + \gamma \Delta p_f)]$$
$$+ \frac{l^3 - a^3}{s^3 K_2} [\Delta \sigma - (\beta \Delta p_2 + \gamma \Delta p_f)] + \frac{s^3 - l^3}{s^3 K_f} (\Delta \sigma - \gamma \Delta p_f) - \frac{a^3}{s^3} \Delta \varepsilon_s. \tag{17}$$

From Eq. (17), the change of fracture porosity can be derived as

$$\frac{\phi_f}{\phi_{f0}} = 1 + \frac{1}{3 K_f} \frac{1}{\frac{a^3}{s^3 K_1} + \frac{l^3 - a^3}{s^3 K_2} + \frac{s^3 - l^3}{s^3 K_f}} \left[\frac{a^3}{s^3} \Delta \varepsilon_s + \Delta \varepsilon_v + \frac{1}{s^3} \frac{a^3}{K_1} (\alpha \Delta p_1 + \beta \Delta p_2) \right.$$
$$\left. + \frac{l^3 - a^3}{s^3 K_2} \beta \Delta p_2 \right]. \tag{18}$$

We then obtain the improved permeability evolution model (IPEM) for triple porosity fractured sorbing media as

$$\frac{k_f}{k_{f0}} = \{ 1 + \frac{1}{3 K_f} \frac{1}{\frac{a^3}{s^3 K_1} + \frac{l^3 - a^3}{s^3 K_2} + \frac{s^3 - l^3}{s^3 K_f}} \left[\frac{a^3}{s^3} \Delta \varepsilon_s + \Delta \varepsilon_v \right.$$
$$\left. + \frac{1}{s^3} \frac{a^3}{K_1} (\alpha \Delta p_1 + \beta \Delta p_2) + \frac{l^3 - a^3}{s^3 K_2} \beta \Delta p_2 \right] \}^3 \tag{19}$$

So far, we have established IPEM for dual porosity and triple porosity fractured sorbing media. The same assumptions are used in the derivation of both permeability models. Next, we will simplify this model and obtain SIPEM1 and SIPEM1-1 for triple porosity fractured sorbing media for later models validation and comparison.

2.4. Model simplification

2.4.1. Replace the volume with the length for each medium (SIPEM1)

Because when the size of the REV and the volumetric strain is small, replacing the volume with the length of each medium will only cause relatively small error. Based on this, the volumetric strain of the REV can be expressed as Eq. (20) for the triple porosity media

$$\Delta \varepsilon_v = \frac{a}{s K_1} [\Delta \sigma - (\alpha \Delta p_1 + \beta \Delta p_2 + \gamma \Delta p_f)] + \frac{c}{s K_2} [\Delta \sigma - (\beta \Delta p_2 + \gamma \Delta p_f)]$$
$$+ \frac{b}{s K_f} (\Delta \sigma - \gamma \Delta p_f) - \frac{a}{s} \Delta \varepsilon_s. \tag{20}$$

Then the dynamic porosity can be expressed as

$$\Delta b = \frac{b}{3 K_f} \Delta \sigma_{ef} = \frac{b}{3 K_f} (\Delta \sigma - \gamma \Delta p_f). \tag{21}$$

The change in effective stress induced fracture deformation can be obtained from

$$\frac{\phi_f}{\phi_{f0}} = 1 + \frac{1}{3 K_f} \frac{1}{\frac{a}{s K_1} + \frac{c}{s K_2} + \frac{b}{s K_f}} \left[\frac{a}{s} \Delta \varepsilon_s + \Delta \varepsilon_v + \frac{1}{s} \left(\frac{a}{K_1} + \frac{c}{K_2} \right) \beta \Delta p_2 \right.$$
$$\left. + \frac{1}{s} \frac{a}{K_1} \alpha \Delta p_1 \right]. \tag{22}$$

Then, the Simplified IPEM, marked as SIPEM1 for the triple porosity fractured sorbing media can be established as

$$\frac{k_f}{k_{f0}} = \left(\frac{\phi_f}{\phi_{f0}} \right)^3$$
$$= \left\{ 1 + \frac{1}{3 K_f} \frac{1}{\frac{a}{s K_1} + \frac{c}{s K_2} + \frac{b}{s K_f}} \left[\frac{a}{s} \Delta \varepsilon_s + \Delta \varepsilon_v + \frac{1}{s} \left(\frac{a}{K_1} + \frac{c}{K_2} \right) \beta \Delta p_2 + \frac{1}{s} \frac{a}{K_1} \alpha \Delta p_1 \right] \right\}^3 \tag{23}$$
.

2.4.2. Replace the volume with the length and consider the effective stress of each medium is the same (SIPEM1-1)

If the impact of mechanical deformation on the permeability is trivial compared to the impact of swelling or shrinking (Wu et al., 2010a), one probably could assume that the effective stress is also the same for each medium. Based on this assumption, the volumetric strain of the REV can be expressed as Eq. (24) for the triple porosity fractured sorbing media

$$\Delta \varepsilon_v = \frac{a}{s K_1} \Delta \sigma_e + \frac{c}{s K_2} \Delta \sigma_e + \frac{b}{s K_f} \Delta \sigma_e - \frac{a}{s} \Delta \varepsilon_s. \tag{24}$$

The dynamic porosity can be written as

$$\frac{\phi_f}{\phi_{f0}} = 1 + \frac{1}{3 K_f} \frac{1}{\frac{a}{s K_1} + \frac{c}{s K_2} + \frac{b}{s K_f}} \left(\frac{a}{s} \Delta \varepsilon_s + \Delta \varepsilon_v \right). \tag{25}$$

Then, the Simplified IPEM, marked as SIPEM1-1 can be established as

$$\frac{k_f}{k_{f0}} = \left(\frac{\phi_f}{\phi_{f0}} \right)^3 = \left[1 + \frac{1}{3 K_f} \frac{1}{\frac{a}{s K_1} + \frac{c}{s K_2} + \frac{b}{s K_f}} \left(\frac{a}{s} \Delta \varepsilon_s + \Delta \varepsilon_v \right) \right]^3. \tag{26}$$

After establishing the fracture permeability evolution models for dual porosity and triple porosity fractured sorbing media, validations are needed. Therefore, in the following, we will show the validations and comparisons of the permeability models for the triple porosity fractured sorbing media.

3. Governing equations

In this section, we provide the equations that govern different physical processes and can be integrated together to numerically solve field problems.

3.1. Deformation of the fractured sorbing media

The deformation characteristics of the reservoir have been widely studied in previous studies (Sang et al., 2016; Wu et al., 2010b; Zhang et al., 2008), and the governing equation of deformation in reservoir due to gas production can be expressed as

$$G u_{i,jj} + \frac{G}{1 - 2v} u_{k,kj} + f_i = -\alpha p_{1,i} - \beta p_{2,i} - r p_{f,i} - K \varepsilon_{s,i} \tag{27}$$

where $G = E/[2(1 + v)]$ is the shear modulus of the rock.

3.2. Gas flow

For the triple fractured sorbing media like shale gas reservoirs, it is believed that only free gas exists in the inorganic matrix and fractures, while both free gas and adsorbed gas exist in organic matrix. Based on the principle of Langmuir isothermal behavior, gas desorbs from the organic matrix pore surface to pore space and is then driven by the pressure drop. As desorption continues, the gas concentration gradient between the bulk and the surface of the organic matrix drives gas diffusion in the solid organic matrix. For the inorganic matrix and

fractures, only free gas exists. Hence, the migration of gas in these two media can be considered as viscous flow and driven by gas pressure gradient.

3.2.1. Gas diffusion in the organic system

We assume that the gas transport in the organic system follows the Fick's law. Since the pore sizes in the organic matrix are of the order of nanometers, Knudsen diffusion should be considered. So the mass balance equation for the gas phase is defined as

$$\frac{\partial m_1}{\partial t} + \nabla(-D_k \nabla m_1) = -Q_{1-2} \tag{28}$$

where D_k is the modified diffusion coefficient in the porous organic matrix. Q_{1-2} is the gas exchange rate from the organic matrix to the inorganic matrix due to diffusion. t is the elapsed time, and the gas mass content m_1 is the quantity of both free gas and adsorbed gas per volume of the organic matrix system. These parameters can be expressed in Eq. (29)–(32) (Lim and Aziz, 1995; Mora and Wattenbarger, 2009; Kumar et al., 2014; Li and Elsworth, 2015).

$$\begin{cases} Q_{1-2} = w_1 D_k (p_1 - p_2) \\ w_1 = \frac{3\pi^2}{a^2} \end{cases} \tag{29}$$

$$m_1 = \rho_{g1}\phi_1 + (1 - \phi_1)\rho_{ga}\rho_s \frac{V_L}{P_1 + P_L} \tag{30}$$

where ρ_g is the gas density, subscript a represents standard conditions.

The modified diffusion coefficient can be written as (Cao et al., 2017; Wang et al., 2009; Javadpour et al., 2007).

$$D_k = \frac{\phi_1}{\tau} \frac{d}{3} \sqrt{\frac{8RT}{\pi Mg}} . \tag{31}$$

where τ is the tortuosity of the organic matrix, d is the diameter of the nanopore.

Due to the low transport properties of gas in organic matrix and the low proportion of organic matrix, we simplify the equation by assuming only the porosity of organic matrix changes during gas extraction. Although this simplification will bring some small errors, it has little effect on the results of this study. Finally, the relationship of modified diffusion coefficient and porosity of organic matrix can be expressed as

$$D_k = D_{k0} \frac{\phi_1}{\phi_{10}} . \tag{32}$$

The porosity of organic matrix and can be expressed as (Sang et al., 2016; Zhang et al., 2008; Detournay and Cheng, 1993; Wang et al., 2012b).

$$\phi_1 = \frac{1}{1 + S_1}[(1 + S_{10})\phi_{10} + (\alpha + \beta + \gamma)(S_1 - S_{10})] \tag{33}$$

where

$$\begin{cases} S_1 = \frac{1}{K_1 N_1}\left[s\varepsilon_v + \left(\frac{a\alpha}{K_1} - N_1\right)p_1 + \left(N_1 - \frac{b}{K_f} - \frac{N_1}{\beta}\right)\beta p_2 + N_1(\gamma - 1)p_f + a\varepsilon_s\right] \\ S_{10} = \frac{1}{K_1 N_1}\left[\left(\frac{a\alpha}{K_1} - N_1\right)p_{10} + \left(N_1 - \frac{b}{K_f} - \frac{N_1}{\beta}\right)\beta p_{20} + N_1(\gamma - 1)p_{f0} + a\varepsilon_{s0}\right] \\ N_1 = \frac{a}{K_1} + \frac{c}{K_2} + \frac{b}{K_f} \end{cases} \tag{34}$$

These equations define how the adsorbed gas diffuses in the organic portion of the composite system.

3.2.2. Gas flow in the inorganic matrix and fracture

We assume that the gas transport in the inorganic matrix and in the fracture follows Darcy's law, so the mass balance equation for the gas phase can be defined as

$$\begin{cases} \frac{\partial m_2}{\partial t} + \nabla(v_{g2}\rho_{g2}) = Q_{1-2} - Q_{2-f} \\ \frac{\partial m_f}{\partial t} + \nabla(v_{gf}\rho_{gf}) = Q_{2-f} + Q_s \end{cases} \tag{35}$$

where Q_{2-f} is the gas exchange rate from the inorganic matrix to the fracture, Q_s is the mass source due to external injection or extraction, v_g represent the Darcy velocity. These parameters can be expressed as (Lim and Aziz, 1995; Mora and Wattenbarger, 2009; Kumar et al., 2014; Li and Elsworth, 2015).

$$\begin{cases} Q_{2-f} = w_2 \frac{k_2}{\mu}(p_2 - p_f) \\ w_2 = \frac{3\pi^2}{(a+c)^2} \end{cases} \tag{36}$$

$$\begin{cases} v_g = -\frac{k}{\mu}\nabla p \\ m = \phi\rho_g \end{cases} . \tag{37}$$

Similar to the organic matrix, the porosity and permeability evolution in the inorganic matrix can also be expressed as (Sang et al., 2016; Zhang et al., 2008; Detournay and Cheng, 1993; Wang et al., 2012b).

$$\phi_2 = \frac{1}{1 + S_2}[(1 + S_{20})\phi_{20} + (\beta + \gamma)(S_2 - S_{20})] \tag{38}$$

$$k_2 = k_{20}\left(\frac{\phi_2}{\phi_{20}}\right)^3 = k_{20}\left[\frac{1 + S_{20}}{1 + S_2} + \frac{(\beta + \gamma)(S_2 - S_{20})}{\phi_{20}(1 + S_2)}\right]^3 \tag{39}$$

where

$$\begin{cases} S_2 = \frac{1}{K_2 N_1}\left[s\varepsilon_v + \frac{a}{K_1}\alpha p_1 + \left(N_1 - \frac{b}{K_f} - \frac{N_1}{\beta}\right)\beta p_2 + N_1(\gamma - 1)p_f + a\varepsilon_s\right] \\ S_{20} = \frac{1}{K_2 N_1}\left[\frac{a}{K_1}\alpha p_{10} + \left(N_1 - \frac{b}{K_f} - \frac{N_1}{\beta}\right)\beta p_{20} + N_1(\gamma - 1)p_{f0} + a\varepsilon_{s0}\right] \end{cases} . \tag{40}$$

This set of equations allows the gas flow in the inorganic matrix and fracture to be calculated.

4. Numerical model description and its validation against field data

In this section, we use the finite element method to solve the equations derived in the previous section and then validate the models against field data.

4.1. Numerical model description

As shown in Fig. 3, we define a production area of 400×400 m², and the radius of the production well is 0.1 m. Due to the symmetry of the configuration, only one-quarter of the production area is simulated. No displacements are allowed on the left side and the bottom side. The top boundary is applied with an overburden stress, $F_y = 38$ MPa, and the right boundary is applied with a horizontal stress, $F_x = 32$ MPa. For gas flow, a constant well bottom hole pressure p_w of 3.45 MPa is applied on the inner boundary of the production well, and no-flow conditions are applied on all the other boundaries. The initial reservoir pressure in the numerical model is 20.3 MPa (Al-Ahmadi and Wattenbarger, 2011). The input parameters are listed in Table 1, most of which are extracted from the literature (Sang et al., 2016; Al-Ahmadi and Wattenbarger, 2011; Mengal, 2010).

4.2. Numerical model validation against field data

Field gas production rate for a horizontal well (Al-Ahmadi and Wattenbarger, 2011) with multistage hydraulic fracturing treatment producing at a constant well pressure are used to verify our models, and
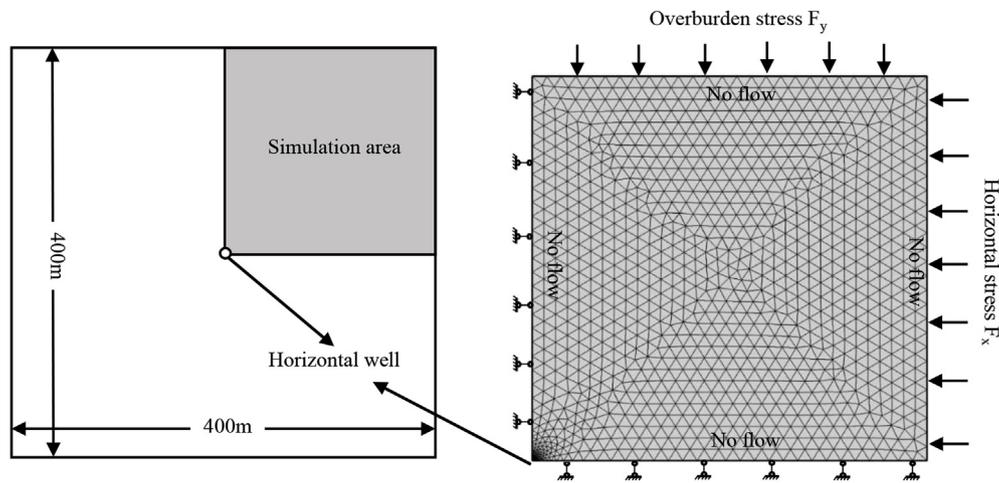
Fig. 3. Numerical model for simulations.

Table 1
Main parameters for case1.

Symbol	Value	Mean and Unit
ε_L	8.1×10^{-4} (Li and Elsworth, 2015)	Langmuir volume strain of CH_4 –
V_L	2.72×10^{-3}	Langmuir volume m^3/kg
P_L	4.48×10^6	Langmuir pressure Pa
T	338.8	Reservoir temperature K
φ_{f0}	0.2	Fracture intrinsic porosity %
k_{f0}	3.9×10^{-17}	Fracture intrinsic permeability m^2
a	1.0×10^{-4}	Organic matrix width m
b	1.0×10^{-5}	Fracture aperture m
c	0.15	Inorganic matrix width m
L	904.6	Horizontal well length m
ν	0.2 (Aadnoy, 2011)	Poisson's ratio –
μ	2.01×10^{-5}	Gas viscosity Pa·s
D_{k0}	1.0×10^{-20} (Etminan et al., 2014)	Diffusion coefficient of CH4 in organic m^2/s
φ_{10}	0.06	Intrinsic porosity of organic matrix –
k_{20}	1.47×10^{-19}	Intrinsic permeability of inorganic matrix m^2
φ_{20}	0.06	Intrinsic porosity of inorganic matrix –
E	3.275×10^{10} (Goodway et al., 2006)	Young's modulus of shale Pa
K_1	3.6×10^9 (Yan and Han, 1949)	Bulk modulus of organic Pa
K_2	2.2×10^{10}	Bulk modulus of inorganic matrix Pa
K_f	1.0×10^8 (Wu et al., 2010b)	Bulk modulus of fracture Pa

the results are shown in Fig. 4. History matching using all three permeability evolution models indicate that model accuracy gets improved from SIPEM1-1 to SIPEM1 to IPEM. Then we adjust $k_2 = 1.47\text{e-}18 \text{ m}^2$ with other parameters unchanged and mark this condition as case2. And we calculate the gas production using IPEM for case2 and then compare with the field data, and the results are shown in Fig. 5a. By comparing Figs. 4c and 5a, the effect of changing the permeability of inorganic matrix on the gas production before 60 days is very small, indicating that the production is mainly controlled by fracture for first 60 days gas production. From the cumulative gas production shown in Fig. 5b we see that the amount of gas produced in the first 60 days accounts for close to 1/5 of the total gas production in 1459 days. This also shows that it is extremely important to accurately describe the evolution of the fracture permeability. Then we verify these models for the period of the first 60 days with field data as shown in Fig. 6. The scatter points are simulation data and field data (Al-Ahmadi and Wattenbarger, 2011), solid lines are trend lines of these data. This figure also shows that IPEM is the best among the three and SIPEM1 is better than SIPEM1-1.

5. Model comparisons

5.1. Comparison of SIPEM1 and SIPEM1-1

In order to more accurately explore the impact of the difference in the effective stress of each medium on fracture permeability evolution, based on case2, we reduce the differences of permeability of each medium, and specific parameters are listed in Table 2. We mark this as case3 and expect the differences in gas pressure and in effective stress between the fracture system and the matrix to be small.

Before analyzing the influence of the difference in effective stress, firstly we calculate how gas pressure evolves at point A (the center point of the simulation area) using the three developed models for case2, and the results are shown in Fig. 7. We can observe that the evolutions of gas pressure in the fracture from the three models are relatively close, therefore we select to use the gas pressure evolution at point A from SIPEM1 as the representative for analysis as shown in Fig. 8. Fig. 8 demonstrates that three stages can be distinguished. In the first stage, the gas pressure in the fracture declines. In the second stage, the gas pressure in the organic matrix declines. After this in the third stage, the gas pressure in the inorganic matrix drops. Fig. 9 shows the evolution of fracture permeability as a function of gas pressure in the fracture corresponding to SIPEM1 and SIPEM1-1, at point A, respectively. Combining Figs. 8 and 9 we can easily find that (1) in the first stage, the evolution of fracture permeability using the two models are almost identical, which would indicate that the pore pressure in different media is not much different, resulting in a small difference in the effective stress in different media. Therefore, the difference of effective stress of each medium at this stage has little effect on the evolution of permeability. (2) In the second stage, the evolution of fracture permeability described by the two models starts to differ gradually. To explain this phenomenon, we need to analyze Fig. 8. In the second stage, on one hand, the gas pressure in the organic matrix decreases which shrinks the organic matrix resulting in an increasing fracture aperture and enhances fracture permeability. On the other hand, the reduction of gas pressure in the fracture increases the effective stress of the reservoir which compresses the fracture and thus reduces the fracture permeability. These two competing processes cause the net fracture permeability to decrease slowly as seen from the SIPEM1. But SIPEM1-1 does not consider the difference of gas pressure in each medium, and the net permeability slightly increases in this stage, therefore the gap between the two models gradually appears. This would also imply that desorption induced strain is relatively large in this stage. (3) In the third stage, the gas pressure in the inorganic matrix starts to decrease and the gas pressure in the organic matrix declines slowly, which would indicate that the increase in effective stress dominates the evolution of
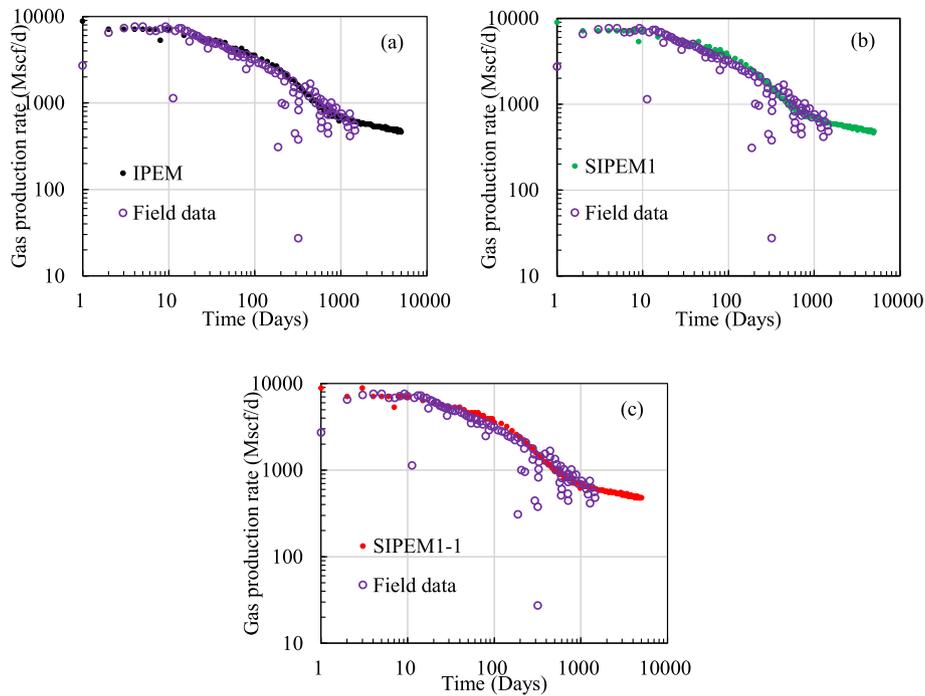
Fig. 4. Log-log plot of simulation results using IPEM (a), SIPEM1 (b), and SIPEM1-1 (c) vs. field data for case1.

fracture permeability in this stage.

The evolution of gas pressure at point A for triple porosity media using SIPEM1 for case3 is shown in Fig. 10. Since the evolution of gas pressure using SIPEM1-1 at point A is also similar to that of SIPEM1, so in this paper we only show the evolution of gas pressure using SIPEM1. Fracture permeability evolutions as a function of gas pressure at point A from SIPEM1 and SIPEM1-1 are shown in Fig. 11. Comparing these two models for case2 and case3, it can be concluded that the gap between SIPEM1 and SIPEM1-1 for case3 is significantly reduced. Comparing Fig. 10 with Fig. 8, it is seen that the difference in pore pressure of each medium is significantly reduced for case3, so that the effective stress difference of each medium is not significant. The underlying assumption for SIPEM1-1 is that compared with the desorption-induced strain, the strain caused by effective stress is negligible, therefore it assumes the effective stress of each medium to be equal. Hence, the evolution of the fracture permeability corresponding to SIPEM1-1 at this period is not significantly different from the fracture permeability evolution described in SIPEM1, which rather precisely considers the effective stress of each medium.

After the above comparative analysis and model validation, we can conclude that, although both SIPEM1 and SIPEM1-1 can describe the field trend of gas production, the error of SIPEM1-1 is relatively larger.
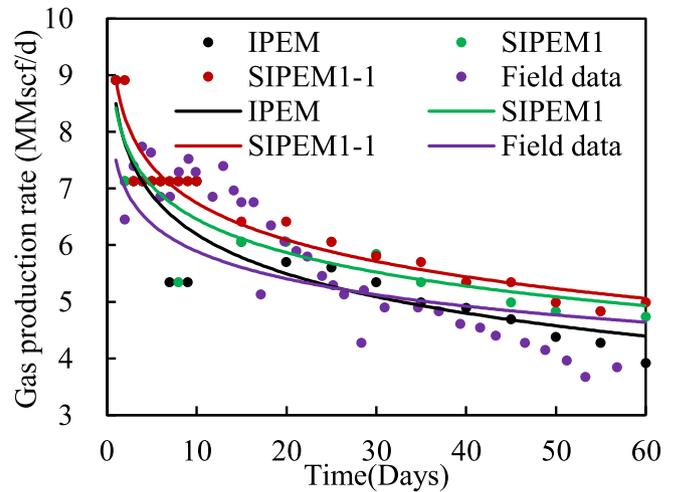
Fig. 6. Simulation results using IPEM, SIPEM1, and SIPEM1-1 vs. field data for the first 60 days production for case1 (scatter points are simulation data and field data, solid lines are trend lines).
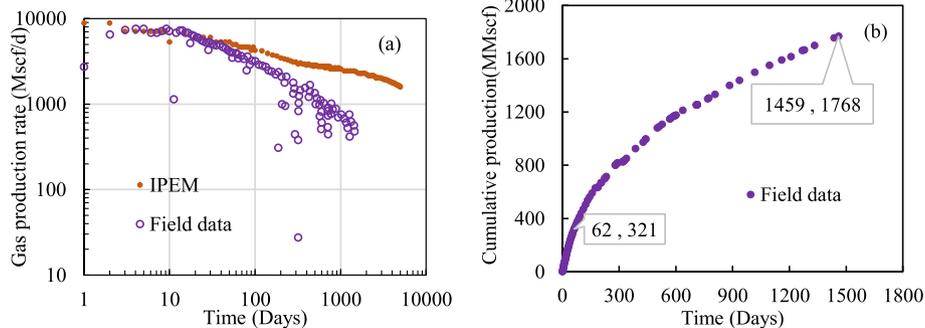
Fig. 5. Log-log plot of simulation results using IPEM for case2 vs. field data (a) and the cumulative production data of the field (b).

Table 2
Parameters for case3.

| Symbol	Value	Mean and Unit
k_{f0}	1.0×10^{-17}	Fracture intrinsic permeability m^2
k_{20}	3.0×10^{-18}	Intrinsic permeability of inorganic matrix m^2
D_{k0}	1.0×10^{-18}	Diffusion coefficient of CH4 in organic matrix m^2/s
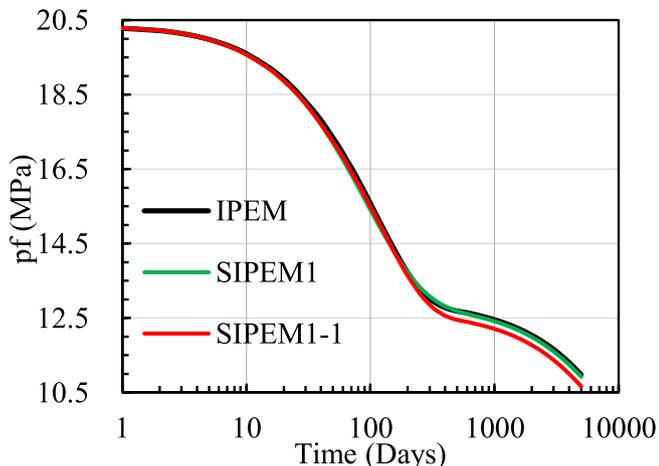
Fig. 7. The gas pressure in fracture varied with time for IPEM, SIPEM1, and SIPEM1-1 under the condition of case2 at point A (the center point of the simulation area).
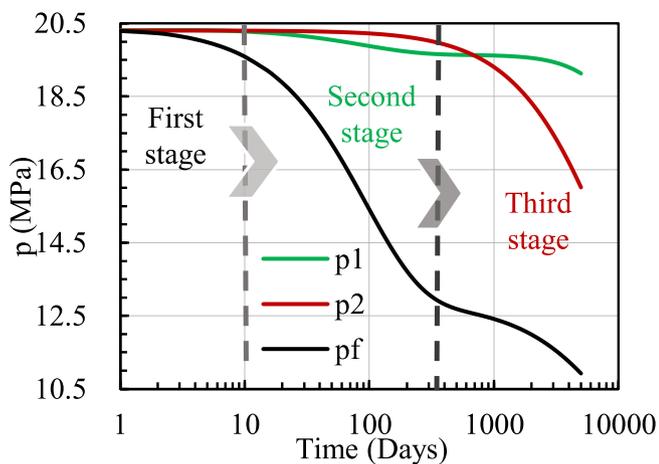
Fig. 8. Gas pressure at point A as a function of time for SIPEM1 for case2.

The gap between the two models is mainly due to the effective stress difference in each medium. The gap between SIPEM1 and SIPEM1-1 will be relatively larger when the permeability difference of each medium is large. And, obviously, this conclusion is also reasonable for the dual porosity fractured sorbing media.

5.2. Comparison of IPEM and SIPEM1

The evolution of fracture permeability at point A corresponding to IPEM and SIPEM1 for case2 is shown in Fig. 12a. We find that the two models almost produce identical results at point A. Therefore, in this study we only show the volumetric strain from SIPEM1, at point A, under conditions of case2 and case4 in Fig. 13 and Fig. 14, respectively. First, we combine the evolution of gas pressure at point A, as shown in Fig. 8, to analyze the volumetric strain of this point under case2 shown in Fig. 13. There are also three noticeable stages: (1) in the first stage gas pressure in fracture begins to decrease, resulting in an increase of
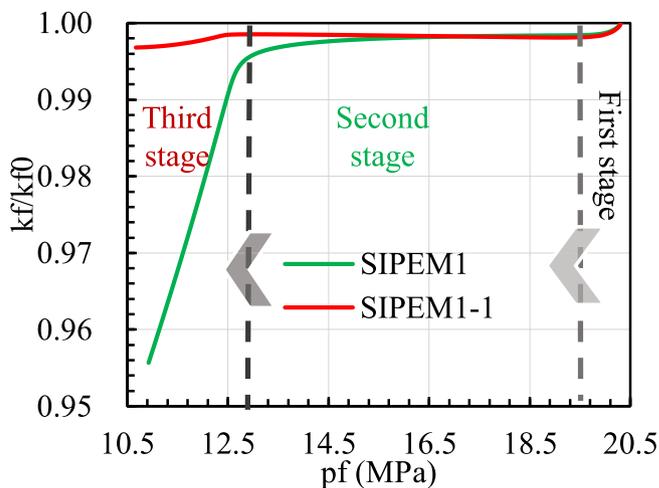
**Fig. 9.** The permeability of fracture at point A for SIPEM1 and SIPEM1-1 for case2.
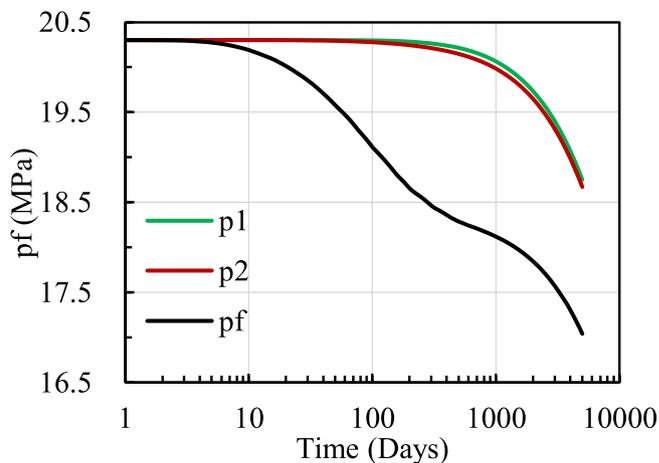
Fig. 10. Gas pressure at point A as a function of time for SIPEM1 for case3.
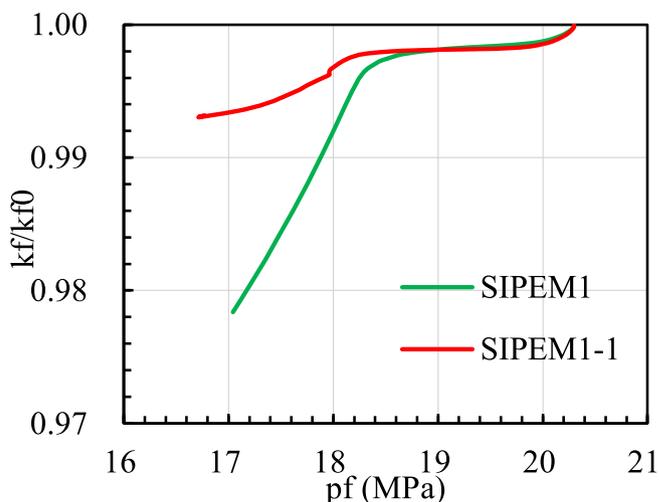

Fig. 11. The permeability of fracture at point A for SIPEM1 and SIPEM1-1 for case3.

the effective stress; (2) in the second stage, gas begins to desorb from the organic matrix, and the gas pressure in the organic matrix decreases. As a result, the organic matrix begins to shrink, which causes the expansion of the inorganic matrix and the fracture, so in this stage,
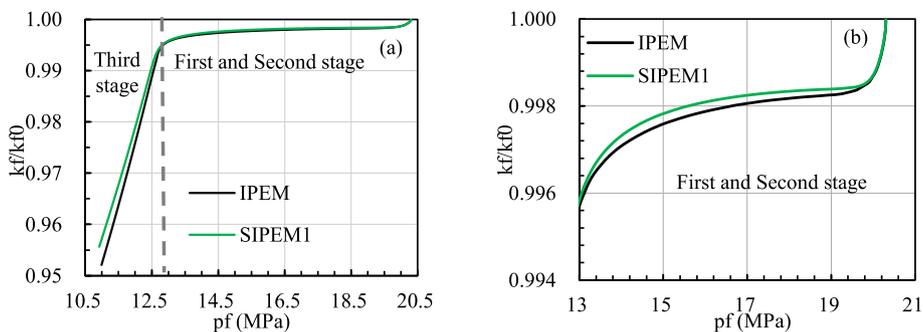
Fig. 12. The permeability of fracture at point A using IPEM and SIPEM1 under case2 for all stages (a), and for only the first and second stage (b).
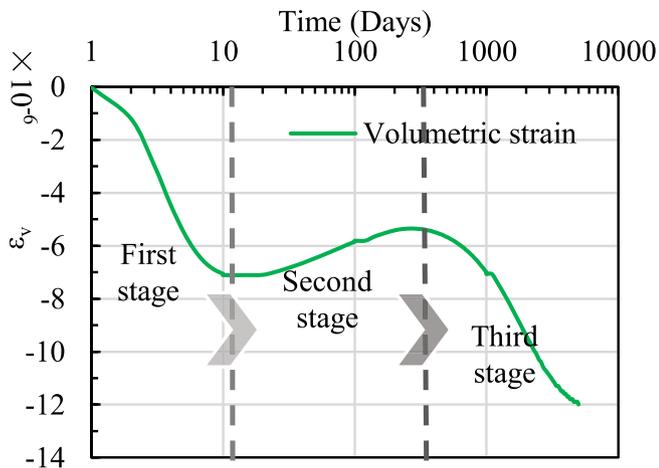

Fig. 13. The volumetric strain at point A as a function of time using SIPEM1 under case2.
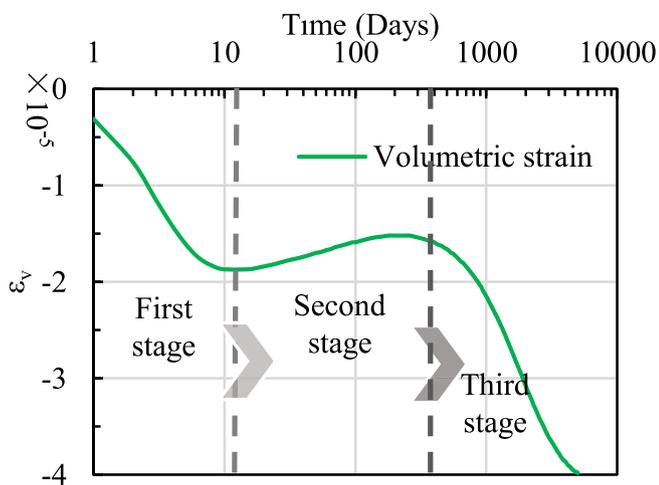

Fig. 14. The volumetric strain at point A as a function of time using SIPEM1 under case4.

although the gas pressure in the fracture decreases rapidly, as we can see from Fig. 13, the net effect on the REV is still a slight expansion; (3) in the third stages, the desorption rate of the gas in the organic matrix is slowed down, and the gas in the inorganic matrix begins to decrease rapidly. As the inorganic matrix accounts for a large proportion of the REV, therefore the REV is rapidly compressed. These three stages clearly reflect the volumetric strain at point A shown in Fig. 13.

Fig. 12b shows the fracture permeability using IPEM and SIPEM1 in the two early stages. It can be seen from this figure that the difference between the permeability of the two models increases first and then

decreases with the decline of gas pressure. This trend corresponds to the volumetric strain at that point as shown in Fig. 13. Because the difference between these two models is that SIPEM1 replaced the volume with the length of each medium, while the IPEM precisely considers the volume. Therefore, it is more appropriate to analyze this phenomenon from the perspective of volumetric strain. In the two early stages, the amount of volumetric strain increases first and decreases later, then in the third stage the volumetric strain of the REV increases rapidly at this point. As a result, the gap between the evolutions of the fracture permeability as described by these two models as shown in Fig. 12 also increases first and decreases later in the two early stages and increases obviously in the third stage.

Next, based on case2, we change the input parameters, listed in Table 3, and record the evolution of the permeability using IPEM and SIPEM1 and mark this as case4. The evolution of the fracture permeability at point A corresponding to these two models under the condition of case4 is shown in Fig. 15. Similar to case2, three stages can be distinguished as shown from Fig. 14. One thing must be noted is that in the second stage of case4, the REV is only slightly expanded, compared to the volumetric strain of this point in this stage under the condition of case2. This phenomenon can be explained by the smaller modulus of the reservoir used under case4, which causes an increase in mechanical strain. This would indicate that the gas desorption induced strain from the organic matrix does not overweight the compression caused by the increase of effective stress.

From the above comparative analysis and model validation, we can conclude that, although both SIPEM1 and IPEM can describe the field trend of gas production, IPEM is better in terms of accuracy. Although IPEM is more complex in terms of mathematic expression, its breadth of application would be greater. In particular, for fractured sorbing media with large compressibility, IPEM can describe permeability evolution behavior more accurately.

6. Conclusions

We have considered the shale gas or coal bed methane reservoir as fractured sorbing media that can be treated as a dual porosity media of matrix-fracture or triple porosity media of organic matrix, inorganic matrix, and fracture. Based on the combined effects of mechanical deformation and desorption induced shrinkage, an improved permeability evolution model for fractured sorbing media were established. Then, we have simplified this model for triple porosity fractured sorbing media,

Table 3
Input parameters used in case4.

| Symbol	Value	Mean and Unit
K_1	3.0×10^9	Bulk modulus of organic Pa
K_2	6.0×10^9	Bulk modulus of inorganic matrix Pa
K_f	3.0×10^7	Bulk modulus of fracture Pa
E	10.0×10^9	Young's modulus of shale Pa
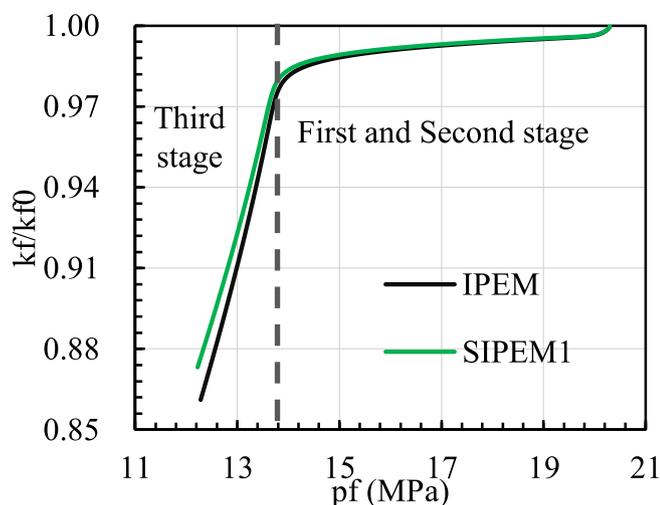
Fig. 15. The permeability of fracture at point A using IPEM and SIPEM1 under case4.

and validated them with field data. Last, we made comparisons among the models under different conditions. The following conclusions can be drawn from this study.

(1) The effect of fracture on reservoir gas production is critical and the most obvious manifestation is in the early production days where the production rates are the highest. Therefore, it is crucial to accurately predict the evolution of permeability of the fracture.

(2) Even though the strain induced by adsorption/desorption is greater than the strain caused by the increase in effective pressure resulting from gas production, we still need to accurately consider the effective stress of different media. If the effective stresses of different media are assumed to be equal, error in permeability evolution would be expected and this would impact the production results from numerical simulations.

(3) Through the comparative analysis between different cases, it can be concluded that although IPEM is mathematically more complex, its breadth of application would be greater. For fractured sorbing media with large compressibility, IPEM can describe the porosity and permeability evolution more accurately.

Acknowledgments

References

Aadnoy, B.S., 2011. Petroleum Rock Mechanics - Drilling Operations and Well Design, vol. 345. pp. 63–76.

Al-Ahmadi, H.A., Wattenbarger, R.A., 2011. Triple-porosity Models: One Further Step towards Capturing Fractured Reservoirs Heterogeneity.

Biot, M.A., 1941. General theory of three-dimensional consolidation. J. Appl. Phys. 12, 155–164.

Cao, P., Liu, J., Leong, Y.-K., 2017. A multiscale-multiphase simulation model for the evaluation of shale gas recovery coupled the effect of water flowback. Fuel 199, 191–205.

Chen, M., Chen, Z., 1999. Effective stress laws for multi-porosity media. Appl. Math. Mech. 20, 1207–1213.

Chilingar, G.V., 1964. Relationship between porosity, permeability, and grain-size distribution of sands and sandstones. Dev. Sedimentol. 1, 71–75.

Cui, G., Liu, J., Wei, M., Shi, R., Elsworth, D., 2018. Why shale permeability changes under variable effective stresses: new insights. Fuel 213, 55–71.

Detournay, E., Cheng, H.D., 1993. 5–Fundamentals of poroelasticity. Anal. Des. Meth. 140, 113–171.

Elsworth, D., Bai, M., 1992. Flow-deformation response of dual-porosity media. J. Geotech. Eng. 118, 107–124.

Elsworth, D., Spiers, C.J., Niemeijer, A.R., 2016. Understanding induced seismicity. Science 354, 1380–1381.

Etminan, S.R., Javadpour, F., Maini, B.B., Chen, Z., 2014. Measurement of gas storage processes in shale and of the molecular diffusion coefficient in kerogen. Int. J. Coal Geol. 123, 10–19.

Goodway, B., Varsek, J., Abaco, C., April, 2006. Practical applications of P-wave AVO for unconventional gas Resource Plays-2: detection of fracture prone zones with Azimuthal AVO and coherence discontinuity. CSEG Recorder 31/4, 52–65.

Gray, 1987. Reservoir engineering in coal seams. SPE Reservoir Eng. 2, 28–34.

Harpalani, S., Schraufnagel, R.A., 1990. Shrinkage of coal matrix with release of gas and its impact on permeability of coal. Fuel 69, 551–556.

Javadpour, F., Fisher, D., Unsworth, M., 2007. Nanoscale gas flow in shale gas sediments. J. Can. Petrol. Technol. 46, 55–61.

Kumar, H., Elsworth, D., Mathews, J.P., Liu, J., Pone, D., 2014. Effect of CO 2 injection on heterogeneously permeable coalbed reservoirs. Fuel 135, 509–521.

Langmuir, I., 2015. The adsorption of gases on plane surfaces of glass, mica and platinum. J. Chem. Phys. 40, 1361–1403.

Li, X., Elsworth, D., 2015. Geomechanics of CO 2 enhanced shale gas recovery. J. Nat. Gas Sci. Eng. 26, 1607–1619.

Lim, K.T., Aziz, K., 1995. Matrix-fracture transfer shape factors for dual-porosity simulators. J. Petrol. Sci. Eng. 13, 169–178.

Liu, H.H., Rutqvist, J., 2010. A new coal-permeability model: internal swelling stress and fracture–matrix interaction. Transport Porous Media 82, 157–171.

Liu, J., Chen, Z., Elsworth, D., Qu, H., Chen, D., 2011. Interactions of multiple processes during CBM extraction: a critical review. Int. J. Coal Geol. 87, 175–189.

Liu, T., Lin, B., Yang, W., 2017. Impact of matrix–fracture interactions on coal permeability: model development and analysis. Fuel 207, 522–532.

Lu, M., Connell, L.D., 2007. A model for the flow of gas mixtures in adsorption dominated dual porosity reservoirs incorporating multi-component matrix diffusion : Part I. Theoretical development. J. Petrol. Sci. Eng. 59, 17–26.

Ma, J., 2015. Review of permeability evolution model for fractured porous media. J. Rock Mech. Geotech. Eng. 7, 351–357.

Mengal, S.A., 2010. Accounting for Adsorbed Gas and its Effect on Production Bahavior of Shale Gas Reservoirs. Texas A & M University.

Middleton, R.S., Gupta, R., Hyman, J.D., Viswanathan, H.S., 2017. The shale gas revolution: barriers, sustainability, and emerging opportunities. Appl. Energy 199, 88–95.

Mora, C.A., Wattenbarger, R.A., 2009. Analysis and verification of dual porosity and CBM shape factors. J. Can. Petrol. Technol. 48, 17–21.

Palmer, I., Mansoori, J., 1998. How permeability depends on stress and pore pressure in coalbeds: a new model. SPE Reservoir Eval. Eng. 1, 539–544.

Robertson, E.P., 2005. Measurement and Modeling of Sorption-induced Strain and Permeability Changes in Coal.

Robertson, E.P., Christiansen, R.L., 2006. A permeability model for coal and other fractured, sorptive-elastic media. SPE J. 13, 314–324.

Sang, G., Elsworth, D., Miao, X., Mao, X., Wang, J., 2016. Numerical study of a stress dependent triple porosity model for shale gas reservoirs accommodating gas diffusion in kerogen. J. Nat. Gas Sci. Eng. 32, 423–438.

Sawyer, W.K., Paul, G.W., Schraufnagel, R.A., 1990. Development and application of a 3-d coalbed simulator. In: Annual Technical Meeting.

Seidle, J.R., Huitt, L.G., 1995. Experimental measurement of coal matrix shrinkage due to gas desorption and implications for cleat permeability increases. In: International Meeting on Petroleum Engineering. Society of Petroleum Engineers, Inc, Beijing, China.

Wang, G.X., Wei, X.R., Rudolph, V., Wei, C.T., Qin, Y., 2009. A multi-scale model for CO2 sequestration enhanced coalbed methane recovery. Front. Chem. Eng. China 3, 20–25.

Wang, S., Elsworth, D., Liu, J., 2012a. A mechanistic model for permeability evolution in fractured sorbing media. J. Geophys. Res.: Solid Earth 117 (n/a-n/a).

Wang, J.G., Kabir, A., Liu, J., Chen, Z., 2012b. Effects of non-Darcy flow on the performance of coal seam gas wells. Int. J. Coal Geol. 93, 62–74.

Warren, J.E., Root, P.J., 1963. The behavior of naturally fractured reservoirs. Soc. Petrol. Eng. J. 3, 245–255.

Wu, Y., Liu, J., Elsworth, D., Miao, X., Mao, X., 2010a. Development of anisotropic permeability during coalbed methane production. J. Nat. Gas Sci. Eng. 2, 197–210.

Wu, Y., Liu, J., Elsworth, D., Chen, Z., Connell, L., Pan, Z., 2010b. Dual poroelastic response of a coal seam to CO2 injection. Int. J. Greenh. Gas Contr. 4, 668–678.

Yan, F., Han, D.H., 1949. Measurement of elastic properties of kerogen. In: Seg Technical Program Expanded, pp. 2778–2782.

Yuan, J., Luo, D., Feng, L., 2015. A review of the technical and economic evaluation techniques for shale gas development. Appl. Energy 148, 49–65.

Zhang, H., Liu, J., Elsworth, D., 2008. How sorption-induced matrix deformation affects gas flow in coal seams: a new FE model. Int. J. Rock Mech. Min. Sci. 45, 1226–1236.

Zou, M., Wei, C., Yu, H., Song, L., 2015. Modeling and application of coalbed methane recovery performance based on a triple porosity/dual permeability model. J. Nat. Gas Sci. Eng. 22, 679–688.